












SAFIIRA: A heavy-ion multi-purpose irradiation facility in Brazil

Cite as: Rev. Sci. Instrum. **91**, 053301 (2020); <https://doi.org/10.1063/1.5138644>

Submitted: 14 November 2019 . Accepted: 10 April 2020 . Published Online: 01 May 2020

V. A. P. Aguiar , N. H. Medina , N. Added, E. L. A. Macchione, S. G. Alberton, A. R. Leite , F. R. Aguirre, R. V. Ribas, C. C. Perego, L. M. Fagundes, J. C. Terassi, J. A. P. Brage, R. F. Simões, O. B. Moraes, E. A. Almeida, P. M. Joaquim, M. S. Souza, A. F. M. Cecotte, R. Martins, J. G. Duarte , V. B. Scarduelli, P. R. P. Allegro, R. Escudeiro, E. Leistenschneider , R. A. N. Oliveira, W. A. Servelo, M. T. Silva, V. E. Sarmiento, C. A. Carreira, J. C. Abreu, S. C. Silva, H. C. Santos, C. L. Rodrigues , R. F. Assis, T. F. Silva , M. H. Tabacniks , A. S. Joaquim, J. H. P. Minas, D. Kashinsky, M. A. Guazzelli , L. E. Seixas , S. Finco, and F. Benevenuti 



View Online



Export Citation



CrossMark

ARTICLES YOU MAY BE INTERESTED IN

[Overview and summary of the 18th International Conference on Ion Sources, Lanzhou, China, 2019](#)



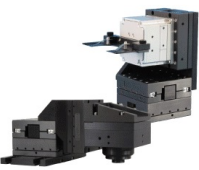
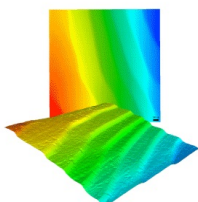
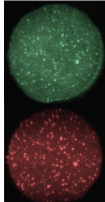
Review of Scientific Instruments **91**, 041601 (2020); <https://doi.org/10.1063/5.0007371>

[Surface temperature estimation in determined multi-wavelength pyrometry systems](#)

Review of Scientific Instruments **91**, 054901 (2020); <https://doi.org/10.1063/5.0005676>

[Forward modeling of Doppler velocity interferometer system for improved shockwave measurements](#)

Review of Scientific Instruments **91**, 043103 (2020); <https://doi.org/10.1063/1.5143246>

 MCL MAD CITY LABS INC. www.madcitylabs.com	<p>Nanopositioning Systems</p> 	<p>Modular Motion Control</p> 	<p>AFM and NSOM Instruments</p> 	<p>Single Molecule Microscopes</p> 
--	--	--	---	--

SAFIIRA: A heavy-ion multi-purpose irradiation facility in Brazil

Cite as: Rev. Sci. Instrum. 91, 053301 (2020); doi: 10.1063/1.5138644

Submitted: 14 November 2019 • Accepted: 10 April 2020 •

Published Online: 1 May 2020



V. A. P. Aguiar,^{1,a)} N. H. Medina,¹ N. Added,¹ E. L. A. Macchione,¹ S. G. Alberton,¹ A. R. Leite,¹ F. R. Aguirre,¹ R. V. Ribas,¹ C. C. Perego,¹ L. M. Fagundes,¹ J. C. Terassi,¹ J. A. P. Brage,¹ R. F. Simões,¹ O. B. Morais,¹ E. A. Almeida,¹ P. M. Joaquim,¹ M. S. Souza,¹ A. F. M. Cecotte,¹ R. Martins,¹ J. G. Duarte,¹ V. B. Scarduelli,¹ P. R. P. Allegro,¹ R. Escudeiro,¹ E. Leistenschneider,¹ R. A. N. Oliveira,¹ W. A. Servelo,¹ M. T. Silva,¹ V. E. Sarmiento,¹ C. A. Carreira,¹ J. C. Abreu,¹ S. C. Silva,¹ H. C. Santos,¹ C. L. Rodrigues,¹ R. F. Assis,¹ T. F. Silva,¹ M. H. Tabacniks,¹ A. S. Joaquim,¹ J. H. P. Minas,¹ D. Kashinsky,¹ M. A. Guazzelli,² L. E. Seixas, Jr.,³ S. Finco,³ and F. Benevenuto⁴

AFFILIATIONS

¹Institute of Physics, University of Sao Paulo, 05508-090 São Paulo, Brazil

²Universitary Center of FEI, 09850-901 São Bernardo do Campo, Brazil

³Information Technology Center, 13069-901 Campinas, Brazil

⁴Federal University of Rio Grande do Sul, 91509-900 Porto Alegre, Brazil

^{a)} Author to whom correspondence should be addressed: vitor.angelo.aguiar@usp.br

ABSTRACT

This work describes the new facility for applied nuclear physics at the University of Sao Paulo, mainly for irradiation of electronic devices. It is a setup composed of a quadrupole doublet for beam focusing/defocusing plus multiple scattering through gold foils to produce low intensity, large-area, and high-uniformity heavy-ion beams from ^1H to ^{107}Ag . Beam intensities can be easily adjusted from 10^2 particles cm^2/s to hundreds of nA for an area as large as 2.0 cm^2 and uniformity better than 90%. Its irradiation chamber has a high-precision motorized stage, and the system is controlled by a LabViewTM environment, allowing measurement automation. Design considerations and examples of use are presented.

Published under license by AIP Publishing. <https://doi.org/10.1063/1.5138644>

I. INTRODUCTION

The increasing use of semiconductor devices for high reliability applications subjected to ionizing radiation has led to the study of the degradation of such systems exposed to different types, energies, doses, and/or fluxes of ionizing radiation.¹ Although the initial concern was related to aerospace applications,¹ the development of more powerful particle accelerators has also shown the need for radiation-tolerant front-end electronics for nuclear and particle physics.²

From encapsulation contaminants to cosmic rays and accelerator-based sources,^{3–5} the investigations of the effects of ionizing radiation on electronic devices were conducted by both research institutions and private companies in order to establish the response of devices to each type of radiation and the development

of mitigation techniques of these effects by means of physical and/or logical design.^{6–8} With the evolution of electronic device technologies and materials, the response to the effects of ionizing radiation can be different, asking for new hardening approaches, thus making this field of research a continuously growing one.

Regarding aerospace applications, satellites over South America are subjected to an increased particle flux (mainly protons) due to the South Atlantic Magnetic Anomaly,⁹ a terrestrial magnetic field deformation that causes higher particle fluxes at lower altitudes. For countries in this region that need operational satellites for communication and territorial monitoring, such satellites must be built with radiation-tolerant electronic devices to ensure long-term operation and reliability.

Outside the domain of semiconductor applications, a heavy-ion beam irradiation facility in the MeV energy range is necessary

to conduct experiments of radiation effects on polymers,¹⁰ ceramics,^{11,12} metals, and alloys,^{13–15} allowing the study of phase changes, modifications in mechanical and optical properties, and the simulation of neutron environments,¹³ as higher particle ranges than those obtained with ion implanters provide a near-constant dose near the material surface. Materials science applications also include ion beam analysis techniques^{16,17} and their damage effects on cultural heritage objects.¹⁸ On the other hand, the development of irradiation facilities opens a wide range of applications, such as radio-biology^{19–21} and the testing of radio-protective drugs.²²

In order to develop studies of radiation effects on materials, mainly in semiconductor electronic devices, the use of appropriate radiation fields ensures data quality, comprehensive experiments, and testing efficiency. In semiconductor devices, the radiation effects of interest and experimental methods for each kind of test are described in Secs. I A and I B.

A. Radiation effects on electronic devices

The ionizing radiation effects on electronic devices can be divided into three main categories: total ionizing dose (TID), displacement damages (DD), and single event effects (SEEs), with TID and DD cumulative effects and SEE stochastic.^{5,23} The most notable differences between these categories are in the energy deposition density and the behavior of the generated charge in the semiconductor.

The total ionizing dose effects are deterministic and related to the total deposited energy during device operation. Although all ionizing radiation can cause TID effects, most considerations deal with photons, electrons, and protons, as their low energy deposition density does not create a high concentration of electron-hole pairs to trigger SEE. The charge generated by radiation is trapped in defects in the SiO₂ layer or at the Si/SiO₂ interface. This charge accumulation may modify the electrical properties of the device.

Displacement damages occur when an impinging particle, a proton, a neutron, or a heavy ion, for example, dislocates an atom of the semiconductor's crystalline structure, thus creating an energy level in the semiconductor bandgap and, therefore, affecting its electrical parameters. On structural materials (metals, alloys, and ceramics), displacement damages can affect mechanical properties.

Single-event effects (SEEs) are stochastic effects caused mainly by heavy-ions due to their high stopping power, which leads to a large quantity of energy deposited through ionization along its path in a semiconductor device. If this energy deposition occurs in a device's sensitive node, a large number of charge carriers may be enough to result in an unexpected signal or even to activate a state of high current that could permanently damage the device.^{5,23} While less frequent, SEE can also be triggered by recoils or nuclear reaction products of proton, neutron, or heavy ion interactions²⁴ or even by direct ionization caused by protons in very sensitive technologies.²⁵

SEE can be divided into destructive and non-destructive effects, and this classification depends mainly on device characteristics. Among the destructive events, the single-event burnout occurs in power devices when an ion creates a charge carrier density large

enough to trigger a permanent conducting channel; the most important non-destructive events are Single-Event Transients (SET), a current pulse generated by deposited energy in the presence of an electric field, and Single (or Multiple) Bit Upsets (SBU-MBU), when a SET modifies the logic state of a bit. From the physics point of view, the modeling of SEE depends not only on device characteristics but also on energy deposition 3D profile and ion impact position in a way that exhaustive experiments in different conditions may significantly improve the models' accuracy.^{26–28}

B. Experimental methods

TID effects are usually studied with photon sources (gamma and x-rays), as well as electron accelerators. Displacement damage investigations are done mainly in neutron and proton irradiation facilities.²³

The most common way of studying SEE is using heavy-ion particle accelerators, although alternative techniques, such as using α or fission fragment sources (such as ²⁴¹Am and ²⁵²Cf) or highly focused lasers to mimic the high-density electron-hole pair creation,²³ are used due to their simplicity compared to an accelerator operation and/or schedule.

As SEE occurrence depends upon energy deposition density, it is common to characterize a device's response as a function of energy deposition per unit along the path in the device (the Linear Energy Transfer—LET), which varies with ion species and energy. For a complete characterization and device qualification for space applications,²⁹ LET values should be as high as 120 MeV cm²/mg, but it is not necessary to investigate charge collection phenomena, structural influence, and testing of mitigation techniques.

There are some standards for radiation testing of SEE using heavy-ion particle accelerators^{29–31} to ensure data without severe accuracy errors and proper comparison between different laboratories. Some recommendations are as follows:

- Low ion flux: for SEE studies, usually between 10² and 10⁵ ions/cm²s. The ion flux should be adjusted according to device readout time.³²
- High coverage area: 1–2 cm diameter beam to cover the entire area of the device and also the beam monitoring system. This is not a crucial characteristic when dealing with small size devices, but mandatory when dealing with large samples Field Programmable Gate Arrays (FPGAs, for example).
- High uniformity: spatial intensity and energy variations should not exceed 10%.
- Long ion ranges: at least 30 μ m of silicon is required by ESA and NASA for device qualification. However, several studies are usually conducted with shorter ranges.

Although these characteristics are also adequate for irradiation of biological materials, there is a need for higher particle fluxes when investigating displacement damages in both electronic devices and structural materials, thus calling for a design that could provide both operation modes.

As the standard configuration of an accelerator for nuclear physics delivers a very intense beam on a small area, it is necessary to modify the beam characteristics. The first SEE studies carried out in Brazil used a Rutherford scattering setup to achieve the desired

characteristics.³³ This setup, however, was not adequate to obtain higher fluxes, and the lack of a sample manipulation system, process automation, better uniformity, and a multi-purpose character for applied nuclear physics led to the development of the SAFI-IRA setup.^{34,35} SAFIIRA design details are presented in Sec. II, its main features in Sec. III, and some applications for irradiation of electronic devices in Sec. IV.

II. SYSTEM DESIGN

To achieve the desired beam enlargement and uniformity, two methods are common: beam defocusing, as in Ref. 36, and multiple scattering by thin foils, as in Refs. 37–39. A defocusing technique is dependent on beam emittance, focusing capability, and collimation systems, allowing us to tune beam intensity and uniformity through better or worse focus. First order ion optics calculations are enough to determine optimal configuration,⁴⁰ but this technique is not practical to easily reduce particle flux to $\sim 10^2$ ions cm^2/s . The multiple scattering method is based on many low-angle scatterings that occur as a particle passes through a target foil. The scattering probability follows a Poisson distribution, and thus, thicker targets have higher scattering probabilities at the cost of elevated beam energy loss and straggling.⁴¹

From the many theoretical descriptions of the particle distribution emerging from a thin target,⁴² the most adequate for the low-energy case is the one developed by Meyer.⁴³ Given that the beam energy (in keV) satisfies the relation $E < 25A_1Z_1^2Z_2^2$, where A_1 and Z_1 are the mass and the atomic number of the projectile and Z_2 the atomic number of the target, Meyer uses classical mechanics to determine the emerging distribution. This result was used by Montenegro *et al.*³⁷ to propose a multiple scattering method to obtain a large and uniform proton beam, where the uniformity coefficient ε_f is defined as the difference between the maximum and minimum probability of a particle hitting a specific area, divided by twice its mean probability [Eq. (1)], and can be calculated given the setup characteristics. Expanding their theoretical expression to any ion, the theoretical value for a given situation is given by Eq. (2) for an incident beam of energy E and $Z = Z_1$, delimited by a collimator of diameter D , scattered through a foil of thickness represented by τ ⁴⁴ and $Z = Z_2$, and observed at a distance R , where $g(\tau)$ is a tabulated function by Meyer,⁴³

$$\varepsilon_f = \frac{P_{\max} - P_{\min}}{2\langle P \rangle}, \quad (1)$$

$$\varepsilon_f = \tanh\left(\frac{2,26 \times 10^7}{Z_1^2 Z_2^2 (Z_1^{2/3} + Z_2^{2/3}) g(\tau)^2} (DE/R)^2\right). \quad (2)$$

Smaller values of ε_f correspond to smaller differences between maximum and minimum values of particle's position probability density function and thus to a more uniform beam. In addition, a relative beam current decrease I/I_0 can be derived from the expressions of uniformity,

$$\frac{I}{I_0} = \frac{2\varepsilon_f}{1 + \varepsilon_f}. \quad (3)$$

Beam optics simulations have shown that the defocusing method was not adequate for reducing the beam intensity to desired levels, given the construction restraints. Calculations using Eqs. (1)–(3) have also shown an insufficient flux reduction in the simulated configurations, despite good uniformity values. To work around these problems, a combination of these two methods is proposed, inspired by Ref. 39 and using the beamline quadrupole doublet as the element responsible for beam focusing/defocusing. A scheme for the mixed-setup is shown in Fig. 1. In this configuration, the set slits + Faraday cup is the first beam monitoring element after the beamline quadrupole. After this set, there are two vacuum chambers, each one containing a set of collimator + gold foil (scatterer). In this way, the beam focusing at the slits results in a diverging beam at the first collimator, which greatly reduces the beam intensity. The first scattering foil is responsible for enlarging once more the beam for a new intensity reduction at the second collimator. The second scattering foil is used then to widen the beam particle distribution and make it uniform.

To determine the best positions to place the Faraday cup, scattering foils and irradiation chamber, and also the foil thicknesses, first-order transport and Monte Carlo simulations using transport of ions in matter (TRIM)⁴¹ were conducted for 50 MeV ^{12}C ions and 70 MeV ^{28}Si . Figure 2 shows the simulated particle distribution at the irradiation plane for 50 MeV ^{12}C ions and both 1.5 mg/cm^2 thick foils, and Figs. 3 and 4 present, respectively, the uniformity and transmittance dependence on foil thicknesses for 50 MeV ^{12}C ions.

As shown in these figures, due to the collimator in front of the second scattering foil, the first foil thickness only influences beam transmittance and the second foil is responsible for the beam uniformization. The transmittance in the defocusing section depends on beam emittance, but it was 5% in this setup. The intensity reduction in sectors II and III is strongly dependent on beam species, energy, and scattering foil thickness. In general, between the two gold foils, transmittance ranges from 14% to 0.1%, and

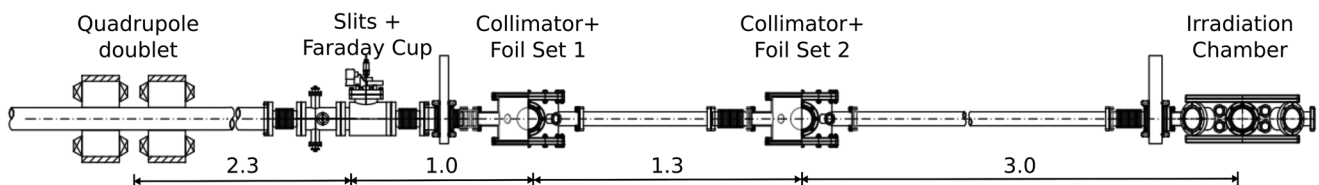


FIG. 1. Schematic drawing of the defocusing-multiple scattering method. Distances in meters.

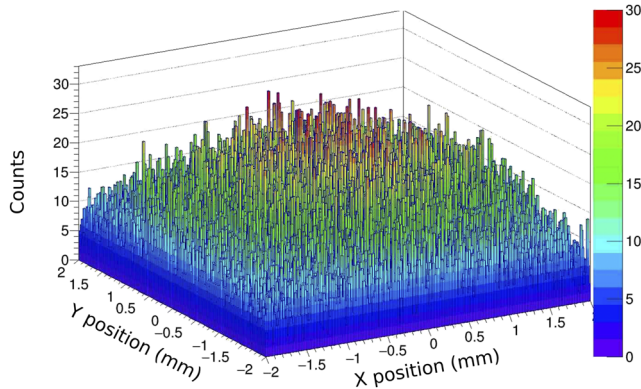
Simulated Beam Profile - ^{12}C 50 MeV

FIG. 2. Simulated particle distribution at the irradiation plane for 50 MeV ^{12}C ions and both gold foils of 1.5 mg/cm^2 .

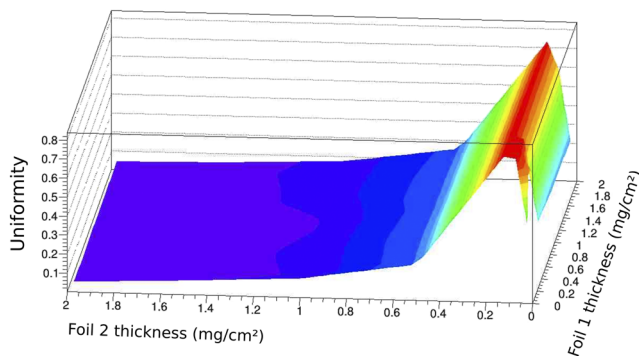
Beam Uniformity - ^{12}C 50 MeV

FIG. 3. Uniformity dependence on gold foil thicknesses for 50 MeV ^{12}C ions.

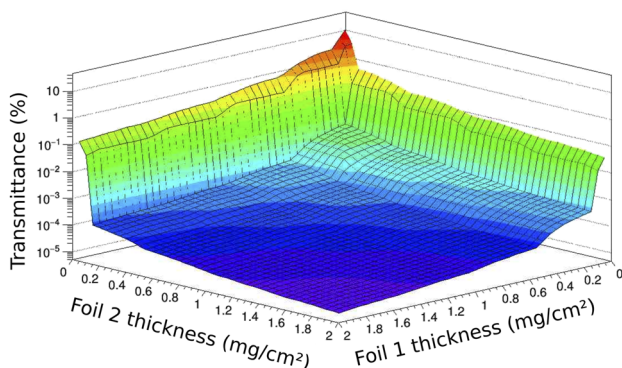
Beam Transmittance - ^{12}C 50 MeV

FIG. 4. Transmittance dependence on gold foil thicknesses for 50 MeV ^{12}C ions. Reprinted with permission from Seixas *et al.*, "New setup for SEE measurements in South America," in 17th European Conference on Radiation and Its Effects on Components and Systems (RADECS). Copyright 2017 IEEE.³⁵

between the second foil and irradiation chamber, it ranges from 82% to 2%.

III. SAFIIRA FACILITY

A. Structure

The facility scheme is shown in Fig. 5. It is installed at the zero-degree beamline in the Nuclear Physics Open Laboratory of University of Sao Paulo (LAFN-USP) in Brazil. The laboratory houses an 8 MV Pelletron accelerator equipped with a cesium sputtering ion source, providing heavy-ion beams from ^1H to ^{107}Ag and energies from 10 MeV to 125 MeV, allowing surface LET values in silicon between 0.02 and $50 \text{ MeV cm}^2/\text{mg}$.

SAFIIRA is composed of three sectors: a focusing sector (I), a scattering sector (II), and an irradiation sector (III). Sector I starts at the laboratory's switching magnet (1) and comprises the quadrupole doublet (2) for beam focusing/defocusing, a pair of trimmers to adjust the beam trajectory (3), an ion pump (4), and the beam diagnostics elements: a wire scanner (5), a four-motorized-slits set (6), and the Faraday cup (7). Sector II starts at the gate valve (8) and is composed of a ceramic insulator (9), a 67 l/s turbo molecular vacuum pump (11), and the two scattering chambers (10 and 12), each one with a set of 1.5 mm Ta collimator and 2 Au scattering foils. In the first chamber, the flux control system composed of a surface barrier detector is also located. The third sector is composed of a gate valve (13), the irradiation chamber (14) and its accessories, a 260 l/s turbo molecular vacuum pump (15), and a port with thin foil for obtaining an external beam (16).

The operation consists in focusing the ion beam in the set slits + Faraday cup; therefore, the beam will be defocused at the first chamber. Changing the focus, it is possible to increase or decrease the ion flux. Each chamber contains two gold foils to scatter the beam, and the choice between them is the compromise between energy loss and flux reduction, for the first set, and energy loss and uniformity, for the second set.

The irradiation chamber (Fig. 6) is a 50 cm diameter stainless steel chamber with six 6" flanges, a 4 1/2" beam exit flange, and several KF flanges. Its main features are

- shielded 50-pin DB, 32 pin circular, and BNC feedthroughs;
- a proportional gas chamber for elastic recoil detection analysis (ERDA) at 45° ;
- a $2.5 \mu\text{m}$ - 1.0° precision 4-axis motorized stage for sample manipulation;
- standard NIM-CAMAC electronics;
- a 1 GHz oscilloscope for device characterization;
- a National Instruments-PCI eXtension for Instrumentation (NI-PXI)³⁵ station for device electrical characterization, sample control, and data acquisition;
- a Mylar beam exit window for in-air irradiations;
- a CCD camera for observation from the control room;
- a ^{241}Am alpha-particle source for low-LET irradiation and off-line device readout testing; and
- surface barrier detectors for flux calibration and RBS analysis.

B. Software control

Several features in the new setup were developed in a LabViewTM environment, allowing process automation and

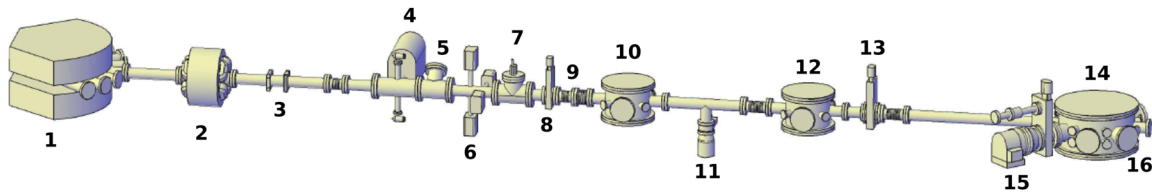


FIG. 5. A schematic (not in scale) view of the new beam line (see text for references). Reprinted with permission from Seixas *et al.*, “New setup for SEE measurements in South America,” in 17th European Conference on Radiation and Its Effects on Components and Systems (RADECS). Copyright 2017 IEEE.³⁵

reproducibility. Serial communication was used for the motorized stage control and a NI-DAQ-MX⁴⁶ module for data acquisition and digital I/O. These tools were used in a spectrum acquisition software, a motion control software, a scanning software, and a slit control software. A NI-FGEN 5406⁴⁷ was used as a configurable digital pulse generator unit.

The spectrum acquisition software consists of four parallel finite state machines (FSMs): the first one is a timer, the second one is a user-interface state machine that waits for a user command (“play,” “stop,” etc.) to send control for the other machines. The third FSM is responsible for normalizer counting (as described in Sec. III C) and for acquiring spectral data and buffering it into an array. The analog value is read from an amplifier output, only when a trigger signal was also received, therefore needing a timing single-channel analyzer. The fourth FSM refreshes the spectra and sums up counts in a given interval. It can be run in free-mode in which data acquisition stops by user command, in fixed-time mode, fixed-counts, or fixed-peak-counts. As the acquisition is stopped, the beamline Faraday cup (no. 7 in Fig. 5) can be automatically inserted for a precise dose control.

The motion control software consists of a loop that configures the last position and data files and waits for the user command. As the command, such as “move to $x = 0$ mm, $y = 2$ mm, $z = 10$ mm,

$\theta = 45^\circ$,” is received, it is processed by a finite state machine responsible for moving x , y , z , and the θ axis, in that order, and saving each new position in recovery files. The final state of the sequence draws the new position on the screen. Sample holder, sample position in it, and pre-defined positions are configurable options.

Scanning software was developed for uniformity characterization and has been used since then for applications. It is a combination of spectrum acquisition and motion control. The whole spectra acquisition is then comprised in one state of the motion control machine after all movements were finished. The configuration step in motion control software includes then the initial and final position setup, step sizes, and stop option (elapsed time or number of counts). Output files include a general file of position–time–counts and detector spectra for each position. A simplified flow chart of the scanning software is shown in Fig. 7.

Slit control software is responsible for NEC motorized slits control⁴⁸ and beam current readout. A pulse generator allows us to insert pulses from -10 V to 10 V up to 10 MHz in any system. It features sine, square, sawtooth, Gaussian (uni and bipolar), delta, fast NIM, and configurable exponential decay pulses to match detector characteristics for instrument testing, dead-time measurement, noise insertion, etc.

C. Flux control

The flux control methodology is the one described in Ref. 39, where its reliability is also shown. It is done employing two silicon surface barrier particle detectors, one placed at an angle (typically 30 – 45°) relative to the first scattering foil—the normalizer (N), and the other one at irradiation position (IR), delimited by a collimator of area A. These two detectors are used to obtain a calibration factor, defined as

$$f = \frac{\text{counts}_{IR}}{A \times \text{counts}_N}. \quad (4)$$

The calibration measurement is done for enough time to obtain a relative uncertainty in f below 5%. For the irradiation procedure, the IR detector is moved away from the target using the motorized stage, and the particle fluence is obtained as the product of the calibration factor f and the counts in the normalizer detector. Real-time response is also shown in the acquisition software for flux monitoring, a special issue when dealing with heavier ions such as Cu or Ag, as in such cases beam intensity may decrease during the experiment.

When the beam flux is changed by focusing/defocusing using quadrupoles located before the laboratory switching magnet, the

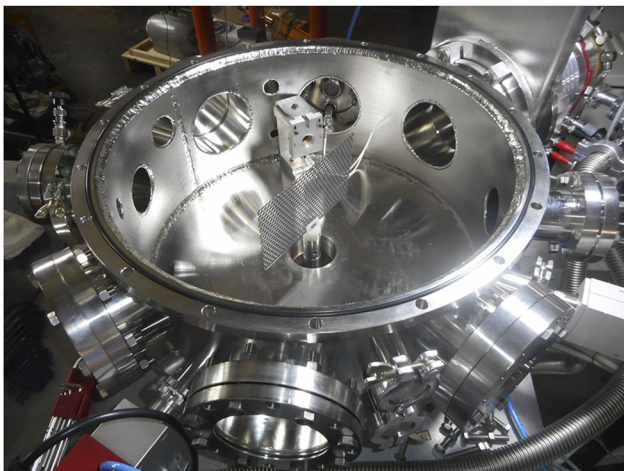


FIG. 6. Internal view of the irradiation chamber with the sample holder attached to the motorized stage.

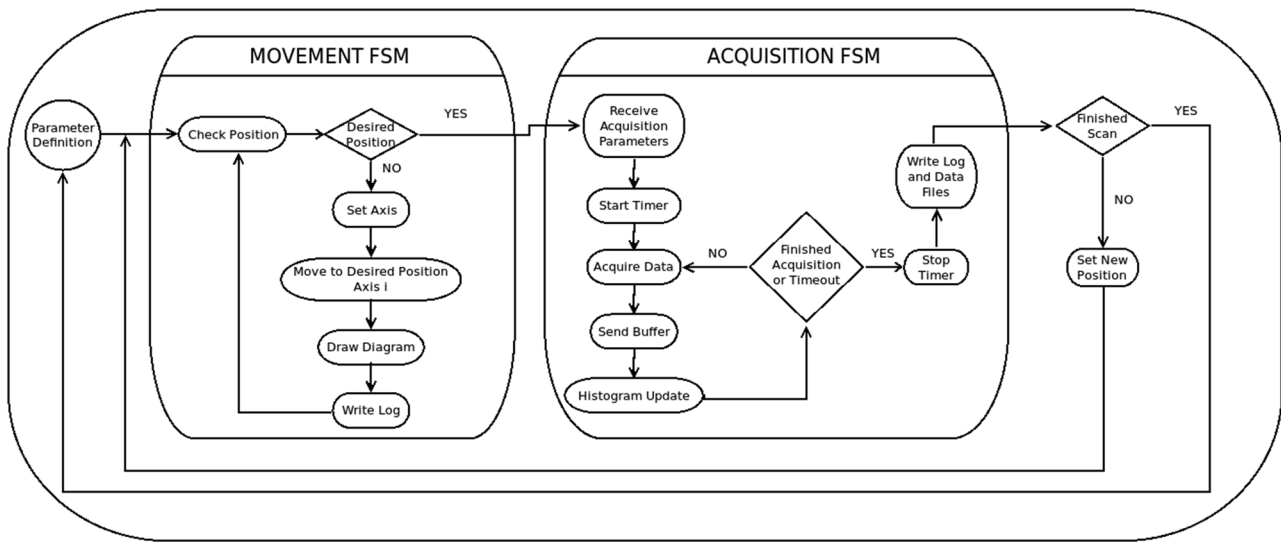


FIG. 7. Flux diagram of scanning software developed in LabView.

calibration factor remains the same up to 10% variation, allowing fast beam tuning.

D. Beam uniformity

Beam uniformity measurements were performed by moving the IR detector with a 0.5 mm collimator in a $2 \times 2 \text{ cm}^2$ area with the aid of the scanning software. Several ion-energy-scatterer combinations were tested. Results are presented in Figs. 8 and 9, normalized by the counts in the detector at the first chamber, and Tables I and II.

As smaller uniformity values ϵ_f represent more uniform beams, these results show that adequate uniformity values for these experiments can be achieved for several heavy-ion beams and energies with

a proper choice of the second scattering foil thickness, allowing the irradiation of samples with area up to 2.0 cm^2 .

IV. APPLICATIONS FOR IRRADIATION OF ELECTRONIC DEVICES

In this section, some of the results for the irradiation of electronic devices obtained in the new beamline are presented. To determine the irradiation position of a fixed sample with respect to a 0.5 mm collimator in the motorized stage, an annular surface barrier silicon detector was placed in front of the sample. Scanning software was then used to find the inner edge of the detector in order to determine the sample irradiation position based on the collimator position. The scanning was done with 1.0 mm steps in the x and y directions, and the results in Fig. 10 show intensity counts in the

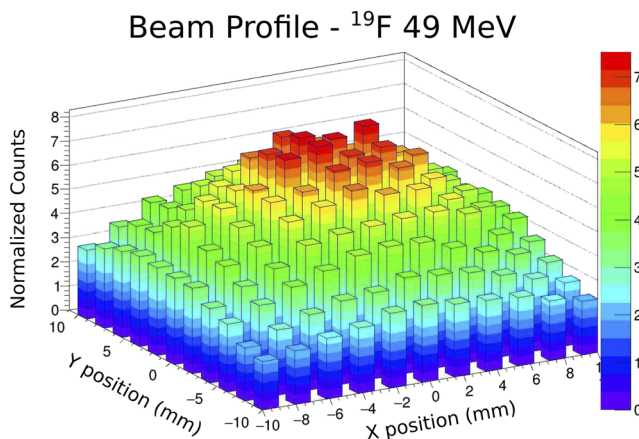


FIG. 8. Normalized particle distribution for 49 MeV ^{19}F ions with gold foil $F_2 = 0.55 \text{ mg/cm}^2$.

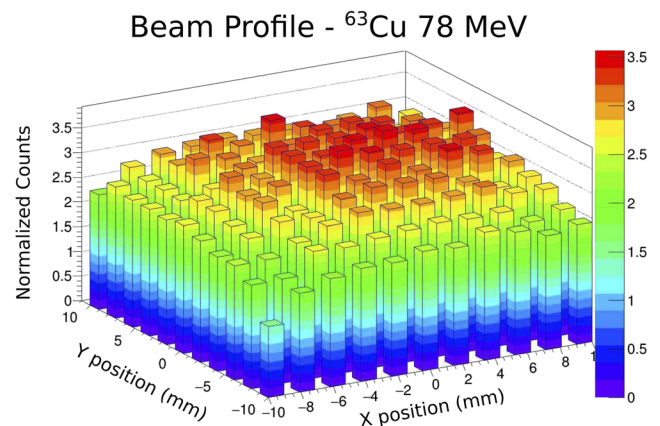


FIG. 9. Normalized particle distribution for 78 MeV ^{63}Cu ions with gold foil $F_2 = 0.65 \text{ mg/cm}^2$.

TABLE I. Uniformity measurements for ^{16}O 42 MeV ion beams and varying second foil thickness.

Second foil thickness (mg/cm^2)	Uniformity
0.65(6)	0.146(9)
1.30(13)	0.0787(20)
0.66(7) ^a	0.096(15)

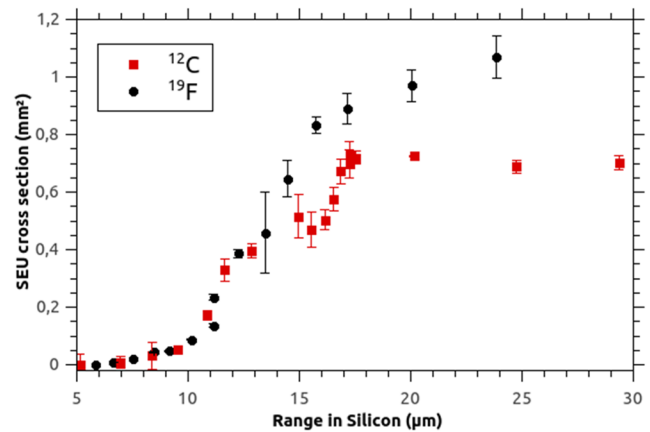
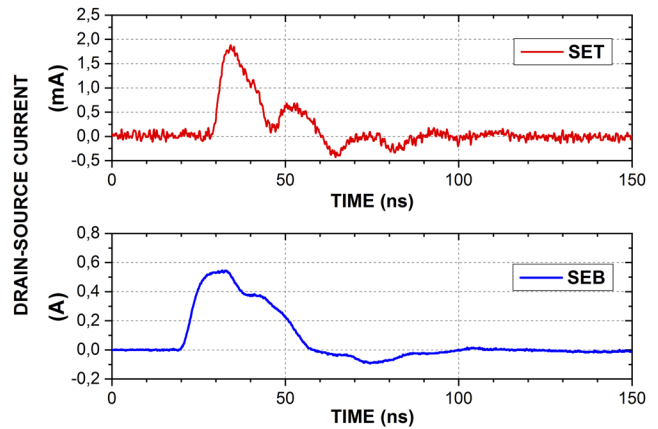
^aUsing just the first foil set.**TABLE II.** Uniformity measurements for several heavy-ion beams and second foil thickness of $0.65 \text{ mg}/\text{cm}^2$.

Ion	Energy (MeV)	Uniformity
^{12}C	35	0.163(16)
^{16}O	35	0.139(22)
^{28}Si	47	0.096(41)
^{35}Cl	42	0.09(5)
^{63}Cu	78	0.05(6)

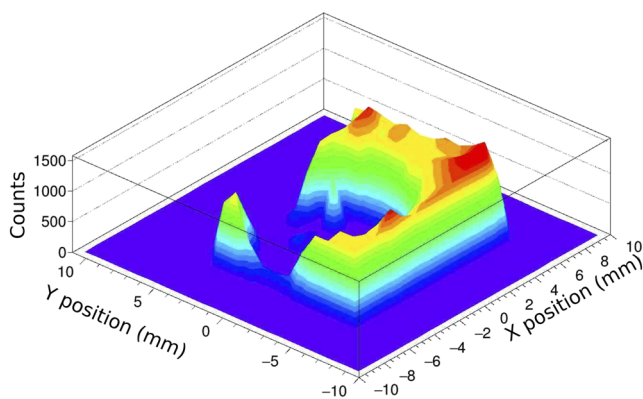
detector as a function of the collimator position. The asymmetry seen in this figure is due to the sample position regarding the center of the scanning area.

Regarding the study of radiation effects on commercial electronic devices, several experiments have been done with analog and digital devices, mainly for single event effect device characterization, mitigation techniques development, and charge collection modeling.^{7,49}

The results of ion beam irradiations on a 28 nm SRAM FPGA are presented in Fig. 11 where the configuration bit-flips were recorded to obtain the single event upset cross section.⁵⁰ The cross section dependence for the ^{12}C and ^{19}F ions reflects the device structure and influence on charge collection. The characteristics of an electrostatic accelerator make it easy to change beam species and/or

**FIG. 11.** Single-event upset cross section as a function of ion range for ^{12}C and ^{19}F ions for energy ranging from 11 MeV to 42 MeV and 21 MeV–53 MeV, respectively.**FIG. 12.** Transient (top) and burnout (bottom) signals observed in an IRLZ34NPBF power transistor under 70 MeV ^{35}Cl ion bombardment.

Annular Detector Profile

**FIG. 10.** Annular surface barrier detector count profile for 49 MeV ^{16}O ions.

energy; in the case of SAFIIRA, the effective beam energy can also be changed by using different sets of scatterer foils, thus increasing beam-time efficiency.

The example of a power MOSFET drain current during heavy-ion irradiation is shown in Fig. 12. Two types of signals are observed: a mA-order transient signal, which can change the transistor logical state, and an A-order signal, which occurs when an avalanche process leads to a high current state that can permanently damage the device.⁵¹

V. CONCLUSIONS

This work describes the new facility for nuclear applied physics at the Nuclear Physics Open Laboratory of University of Sao Paulo, named SAFIIRA, currently in use by several research groups for ion beam irradiations of electronic devices and material analysis. It was designed using beam optics and multiple scattering methods to

deliver ion beams of high uniformity and fluxes ranging from 10^2 to 10^6 particles/cm²s for low dose irradiations and up to nanoamperes (with collimators) or hundreds of nA (without collimators) for high-dose irradiations or material analysis. System control and automation under LabView, the possibility of in-air irradiations, fast beam tuning, and a broad range of ion beams, energies, and LET values are some of the main characteristics that make this facility a turning point in the research of radiation effects in electronic devices and other materials.

ACKNOWLEDGMENTS

We wish to acknowledge Professor Dr. Wayne A. Seale for the English revision of this manuscript and Brazilian funding agencies FAPESP (Project No. 2012/03383-5), FINEP (Project No. 01.12.0244.00), CNPq, and CNEN for financial support.

REFERENCES

- ¹E. Petersen, *Single Event Effects in Aerospace*, 1st ed. (Wiley, 2011).
- ²C. Leroy and P.-G. Rancoita, *Principles of Radiation Interaction in Matter and Detection*, 2nd ed. (World Scientific, 2009).
- ³D. F. Heidel, K. P. Rodbell, E. H. Cannon, C. Cabral, M. S. Gordon, P. Oldiges, and H. H. K. Tang, "Alpha-particle-induced upsets in advanced CMOS circuits and technology," *IBM J. Res. Dev.* **52**, 225–232 (2008).
- ⁴A. Ganguly, S. S. Nath, and M. Choudhury, "Enhanced efficiency in swift heavy ion irradiated CdS quantum dots sensitized solar cell," *IEEE Photonics Technol. Lett.* **30**, 1735–1738 (2018).
- ⁵S. Duzellier, "Radiation effects on electronic devices in space," *Aerosp. Sci. Technol.* **9**, 93–99 (2005).
- ⁶K. Cirne, M. Silveira, R. Santos, S. Gimenez, M. Barbosa, M. Tabacniks, N. Added, N. Medina, W. D. Melo, L. E. Seixas, Jr., and J. D. Lima, "Comparative study of the proton beam effects between the conventional and Circular-Gate MOSFETs," *Nucl. Instrum. Methods Phys. Res., Sect. B* **273**, 80–82 (2011).
- ⁷L. A. Tambara, F. L. Kastensmidt, P. Rech, F. Lins, N. H. Medina, N. Added, V. A. P. Aguiar, and M. A. G. Silveira, "Reliability-performance analysis of hardware and software co-designs in SRAM-based APSOCs," *IEEE Trans. Nucl. Sci.* **65**, 1935 (2018).
- ⁸L. A. Tambara, J. Tonfat, A. Santos, F. L. Kastensmidt, N. H. Medina, N. Added, V. A. P. Aguiar, F. Aguirre, and M. A. G. Silveira, "Analyzing reliability and performance trade-offs of HLS-based designs in SRAM-based FPGAs under soft errors," *IEEE Trans. Nucl. Sci.* **64**, 874 (2017).
- ⁹C. A. Federico, O. L. Gonçalves, E. S. Fonseca, I. M. Martin, and L. V. E. Caldas, "Neutron spectra measurements in the South Atlantic anomaly region," *Radiat. Meas.* **45**, 1526–1528 (2010).
- ¹⁰"Space systems: Space environment: Simulation guidelines for radiation exposure of non-metallic materials," Technical Report No. 15856, ISO, 2010.
- ¹¹B. M. Clark, P. Tumurgoti, S. K. Sundaram, J. W. Amoroso, J. C. Marra, V. Shutthanandan, and M. Tang, "Radiation damage of hollandite in multiphase ceramic waste forms," *J. Nucl. Mater.* **494**, 61–66 (2017).
- ¹²G. P. Pells, "Radiation effects and damage mechanisms in ceramic insulators and window materials," *J. Nucl. Mater.* **155-157**, 67–76 (1988).
- ¹³Gary S. Was, *Fundamentals of Radiation Materials Science* (Springer, 2017).
- ¹⁴M. W. Ullah, Y. Zhang, N. Sellami, A. Debelle, H. Bei, and W. J. Weber, "Evolution of irradiation-induced strain in an equiatomic NiFe alloy," *Scr. Mater.* **140**, 35–39 (2017).
- ¹⁵E. Levo, F. Granberg, C. Fridlund, K. Nordlund, and F. Djurabekova, "Radiation damage buildup and dislocation evolution in Ni and equiatomic multicomponent ni-based alloys," *J. Nucl. Mater.* **490**, 323–332 (2017).
- ¹⁶C. Jeynes, M. J. Bailey, N. J. Bright, M. E. Christopher, G. W. Grime, B. N. Jones, V. V. Palitsin, and R. P. Webb, "Total IBA - where are we?," *Nucl. Instrum. Methods Phys. Res., Sect. B* **271**, 107–118 (2012).
- ¹⁷*Ion Beams for Materials Analysis*, edited by J. R. Bird and J. S. Williams (Academic Press, 1989).
- ¹⁸A. Zucchiatti and F. Agulló-Lopez, "Potential consequences of ion beam analysis on objects from our cultural heritage: An appraisal," *Nucl. Instrum. Methods Phys. Res., Sect. B* **278**, 106–114 (2012).
- ¹⁹J. Kappke, E. R. d. Silva, H. R. Schelin, S. A. Paschuk, A. Pashchuk, A. d. Oliveira, N. Carlin Filho, E. M. Szanto, J. Takahashi, and J. C. d. Souza, "Evaluation of *Escherichia coli* cells damages induced by ultraviolet and proton beam irradiation," *Braz. J. Phys.* **35**, 805–807 (2005).
- ²⁰X. Xu, B. Liu, L. Zhang, and Y. Wu, "Mutagenic effects of heavy ion irradiation on rice seeds," *Nucl. Instrum. Methods Phys. Res., Sect. B* **290**, 19–25 (2012).
- ²¹S. Ritter and M. Durante, "Heavy-ion induced chromosomal aberrations: A review," *Mutat. Res.* **701**, 38–46 (2010).
- ²²A. H. Haskins, D. J. Buglewicz, H. Hirakawa, A. Fujimori, Y. Aizawa, and T. A. Kato, "Palmitoyl ascorbic acid 2-glucoside has the potential to protect mammalian cells from high-LET carbon-ion radiation," *Sci. Rep.* **8**, 13822 (2018).
- ²³J. R. Schwank, M. R. Shaneyfelt, and P. E. Dodd, "Radiation hardness assurance testing of microelectronic devices and integrated circuits: Radiation environments, physical mechanisms and foundations for hardness assurance," Document 2008-6851P, Sandia National Laboratories, 2008.
- ²⁴F. Wrobel, J.-M. Palau, M.-C. Calvet, O. Bersillon, and H. Duarte, "Simulation of nucleon-induced nuclear reactions in a simplified SRAM structure: Scaling effects on SEU and MBU cross sections," *IEEE Trans. Nucl. Sci.* **48**, 1946–1952 (2001).
- ²⁵K. P. Rodbell, D. F. Heidel, H. H. K. Tang, M. S. Gordon, P. Oldiges, and C. E. Murray, "Low-energy proton-induced single-event-upsets in 65 nm node, silicon-on-insulator, latches and memory cells," *IEEE Trans. Nucl. Sci.* **54**, 2474–2479 (2007).
- ²⁶J. Liu, S. Yan, J. Xue, and Y. Wang, "Comparison of ionization track structure models for electronic devices of different sizes," *Nucl. Instrum. Methods Phys. Res., Sect. B* **444**, 43–49 (2019).
- ²⁷A. V. Sogoyan, A. I. Chumakov, A. A. Smolin, A. V. Ulanova, and A. B. Boruzdina, "A simple analytical model of single-event upsets in bulk CMOS," *Nucl. Instrum. Methods Phys. Res., Sect. B* **400**, 31–36 (2017).
- ²⁸J. G. Lopez, M. Jimenez-Ramos, M. Rodriguez-Ramos, J. Forneris, and J. Ceballos, "An upgraded drift-diffusion model for evaluating the carrier lifetimes in radiation-damaged semiconductor detectors," *Nucl. Instrum. Methods Phys. Res., Sect. B* **371**, 294–297 (2016).
- ²⁹ESA, Single event effects test method and guidelines, ESA/SCC Basic Specification 1, European Space Agency, 1995, ESA/SCC Basic Specification 25100.
- ³⁰ASTM, Standard Guide for the Measurement of Single Event Phenomena (SEP) Induced by Heavy Ion Irradiation of Semiconductor Devices, ASTM Standard, American Society for Testing and Materials, 2006, F 1192-00.
- ³¹EIA/JEDEC, Test procedures for the measurement of single-event effects in semiconductor devices from heavy ion irradiation, EIA/JEDEC Standard, Electronic Industries Association, 1996, EIA/JESD57.
- ³²ESA, Total dose steady-state irradiation test method, ESA/SCC Basic Specification 1, European Space Agency, 1995, ESA/SCC Basic Specification 22900.
- ³³V. A. P. Aguiar, N. Added, N. H. Medina, E. L. A. Macchione, M. H. Tabacniks, F. R. Aguirre, M. A. G. Silveira, R. B. B. Santos, and L. E. Seixas, Jr., "Experimental setup for single event effects at the São Paulo 8UD Pelletron accelerator," *Nucl. Instrum. Methods Phys. Res., Sect. B* **332**, 397–400 (2014).
- ³⁴Sistema de Feixes Iônicos para Irradiação e Aplicações.
- ³⁵V. A. P. Seixas, N. H. Medina, N. Added, E. L. A. Macchione, S. G. Alberton, A. Leite, and M. A. Guazzelli, "New setup for SEE measurements in South America," in *2017 17th European Conference on Radiation and Its Effects on Components and Systems (RADECS)*, 2017.
- ³⁶J. Wyss, D. Bisello, and D. Pantano, "SIRAD: An irradiation facility at the LNL tandem accelerator for radiation damage studies on semiconductor detectors and electronic devices and systems," *Nucl. Instrum. Methods Phys. Res., Sect. A* **462**, 426–434 (2001).
- ³⁷E. C. Montenegro, G. B. Baptista, C. V. Barros Leite, A. G. de Pinho, and A. S. Paschoa, "Study of a proton beam diffusing system for PIXE analysis," *Nucl. Instrum. Methods* **164**, 231–234 (1979).
- ³⁸M. Belli, R. Cherubini, G. Galeazzi, S. Mazzucato, G. Moschini, O. Saporita, G. Simone, and M. A. Tabocchini, "Proton irradiation facility for radiobiological

studies at a 7 MV van de Graaf accelerator,” *Nucl. Instrum. Methods Phys. Res., Sect. A* **256**, 576–580 (1987).

³⁹N. Carlin, J. C. de Souza, E. M. Szanto, J. C. Acquadro, E. Okuno, J. Takahashi, N. K. Umisedo, F. J. de Oliveira Filho, and J. A. C. Vasconcelos, “Irradiation facility for radiobiological and molecular biophysics studies at the university of são paulo pelletron accelerator laboratory,” *Nucl. Instrum. Methods Phys. Res., Sect. A* **540**, 215–221 (2005).

⁴⁰M. S. Livingston and J. P. Blewett, *Particle Accelerators* (McGraw-Hill Book Company, 1962).

⁴¹J. F. Ziegler, J. P. Biersack, and M. D. Ziegler, *SRIM: The Stopping and Range of Ions in Matter* (SRIM Co., 2008).

⁴²W. T. Scott, “The theory of small-angle multiple scattering of fast charged particles,” *Rev. Mod. Phys.* **35**, 231–313 (1963).

⁴³L. Meyer, “Plural and multiple scattering of low-energy heavy particles in solids,” *Phys. stat. sol.* **44**, 253–268 (1971).

⁴⁴ τ is a function of foil thickness, projectile atomic number, and target’s atomic number and atomic mass.³⁷

⁴⁵NI-PXIE-8135 datasheet.

⁴⁶NI-PXIE-6259 datasheet.

⁴⁷NI-PXIE-5406 datasheet.

⁴⁸Instruction Manual No. 2ET0384420 for Operation and Service of Remote Slit Drive System.

⁴⁹A. B. de Oliveira, G. S. Rodrigues, F. L. Kastensmidt, N. Added, E. L. A. Macchione, V. A. P. Aguiar, N. H. Medina, and M. A. G. Silveira, “Lockstep dual-core ARM A9: Implementation and resilience analysis under heavy ion-induced soft errors,” *IEEE Trans. Nucl. Sci.* **65**, 1783–1790 (2018).

⁵⁰V. A. P. Aguiar, N. H. Medina, N. Added, E. L. A. Macchione, S. G. Alberton, C. L. Rodrigues, T. F. Silva, G. S. Zahn, F. A. Genezini, M. Morales, F. Benevenuti, and M. A. Guazzelli, “Thermal neutron induced upsets in 28 nm sram,” *J. Phys.: Conf. Ser.* **1291**, 012025 (2019).

⁵¹S. G. Alberton, N. H. Medina, N. Added, V. A. P. Aguiar, R. Menegasso, E. L. A. Macchione, and M. A. G. Silveira, “Single-event effects: Experimental setup for power MOSFETS and diffusion model for cross section calculations in low-voltage MOSFETS,” *J. Phys.: Conf. Ser.* **1291**, 012045 (2019).